PERGAMON

International Journal of Solids and Structures 39 (2002) 297–310

INTERNATIONAL JOURNAL OF SOLIDS and STRUCTURES

www.elsevier.com/locate/ijsolstr

Smooth static and dynamic indentation of a cantilever beam

Minggang Zhou [a], William P. Schonberg [b,*]

[a] *Department of Civil and Environmental Engineering, University of Alabama in Huntsville, Huntsville, AL 35899, USA*
[b] *Department of Civil Engineering, University of Missouri-Rolla, Butler Carlton Hall Rm. 119A, 1870 Miner Circle, Rolla, MO 65409, USA*

Received 6 July 2001; in revised form 28 August 2001

Abstract

The static and dynamic indentation of structural elements such as beams and plates continue to be intriguing problems, especially for scenarios where large area contacts are expected to occur. Standard methods of indentation analyses use a beam theory solution to obtain an overall load–displacement relationship and then a Hertzian contact solution to calculate local stresses under the indenter. However, these techniques are only applicable in a fairly limited class of problems: the stress distribution in the contact region will differ significantly from a Hertzian one when the contact length exceeds the thickness of the beam. The indentation models developed herein are improvements over existing GLOBAL/LOCAL models for static and dynamic indentation of cantilever beams. Maximum contact stresses, beam displacements, and contact force time histories are obtained and compared with the predictions of current static and dynamic indentation models. The validity of the solutions presented herein is further assessed by comparing the results obtained to the predictions of modified beam theory solutions.

Keywords: Static indentation; Non-Hertzian contact; Low velocity impact; Cantilever beam; GLOBAL/LOCAL

1. Introduction

In this paper, we present improved solutions to the frictionless static and dynamic cylindrical indentation problems for a cantilever beam of length L and thickness h (see Fig. 1). Such configurations can serve as first-order models for gear interaction or for turbine blade and hammer impact problems. Standard methods of static and dynamic indentation analyses use a beam theory solution to obtain an overall load–displacement relationship and then a Hertzian contact solution to calculate local stresses under the indenter. However, previous modeling efforts have shown that the stress distribution in the contact region will differ significantly from a Hertzian one when the contact length exceeds the thickness of the beam. In such cases, point contact can no longer be assumed and Hertzian relations are not valid.

While the dynamic indentation problem (i.e. the low velocity impact problem) for a cantilever beam has yet to be solved, static problems of this type were solved previously by Keer and Schonberg (1986a,b) using a

* Corresponding author. Tel.: +1-573-341-4787; fax: +1-573-341-4729.
E-mail address: wschon@umr.edu (W.P. Schonberg).

0020-7683/01/$ - see front matter
PII: S0020-7683(01)00212-8

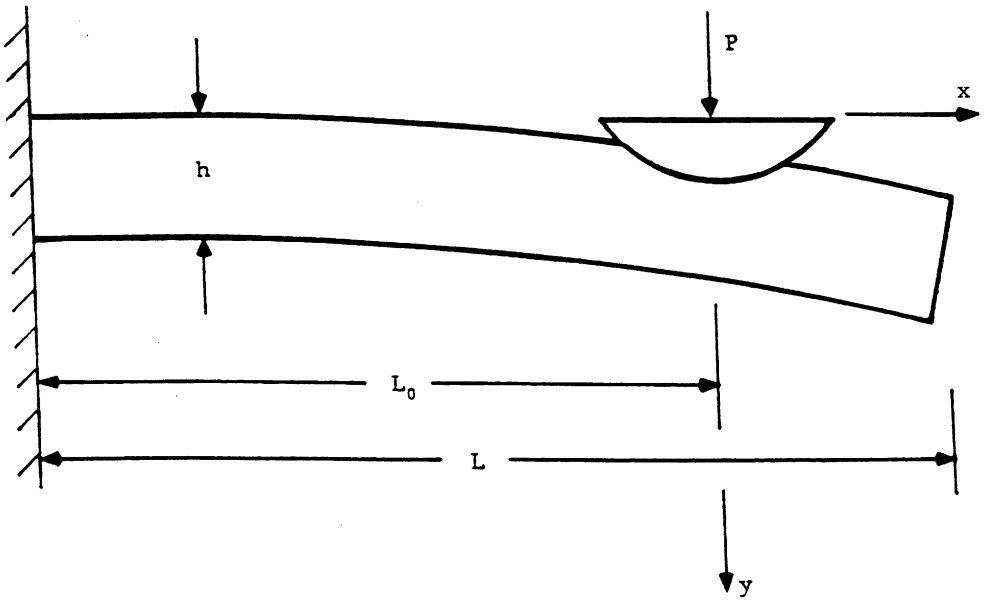

Fig. 1. Indentation of a cantilever beam.

GLOBAL/LOCAL approach that superposed beam theory and elasticity expressions. The technique developed was subsequently modified to include beam rotation effects under the indenter by Zhou and Schonberg (1995). However, these procedures used an approximate solution (instead of an elasticity solution) to establish the load–displacement relationship at the contact site. As a result, because of the way in which they were constructed, these models are incapable of accurately predicting the stress fields inside the finite layer.

In the first part of this paper we present a static indentation model for cantilever beams that is an improvement of current GLOBAL/LOCAL models because it uses a layer solution that is a true elasticity solution to describe the load–displacement relationship at the contact site. Additionally, in a manner similar to Zhou and Schonberg (1995), the rotation of the beam under the indenter is included in the mixed boundary conditions at the contact site. Maximum contact stress values are obtained and compared with the predictions of previously developed GLOBAL/LOCAL static indentation models. The validity of the solutions presented is assessed by comparing the results obtained to the predictions of modified beam theory solutions.

In the second part of this paper, we present a new low velocity impact model for cantilever beams. In this model, the static elasticity solution for a finite elastic layer is merged with a dynamic beam theory solution. Using the composite solution to match boundary conditions leads to a Volterra integral equation of the second kind that is solved incrementally for the unknown pressure and contact length as functions of time. The validity of the solution technique presented is again assessed by comparing its predictions against those of dynamic beam theory solutions.

2. Generalized elasticity solution for a finite layer

The first step in developing the static and dynamic indentation models is to obtain the solution for a finite elastic layer of thickness h and length L that is subjected to an arbitrary upper surface pressure distribution (see again Fig. 1). In subsequent sections, appropriate end conditions are applied to this solution to obtain

the elasticity solutions for the static and dynamic indentation of a cantilever beam. The required solution is achieved by the superposition of an elasticity solution for an infinite layer having a normal load on its upper surface and zero load on its lower surface (see, e.g., Keer and Miller, 1983) and an elasticity solution for a finite layer subjected to asymmetric bending obtained from Airy stress function solutions for asymmetric bending and pure shear (see Zhou and Schonberg, 1995). The final solution is written in terms of two unequal end moments M_0 and M_1 that are applied at $x = -L_0$ and at $x = L_1 = L - L_0$, respectively, and three (as yet) unknown constants a_0, b_0, and a_1 and is presented in Zhou and Schonberg (2001). It is referred to as the *generalized elasticity solution for the finite layer*.

3. Static indentation of a cantilever beam

The mixed boundary value problem to be solved in this section is that of a cantilevered elastic finite length layer of thickness h and length L that is indented by a cylindrical punch on its upper surface (see Figs. 1 and 2). The solution of the problem is achieved by application of the mixed boundary conditions at contact site and the end support conditions to the generalized elasticity solution discussed in the preceding section. As in Zhou and Schonberg (1995), the displacement boundary condition at contact site is written as follows:

$$u_y(x,0) = \Delta + \theta_0 x - \frac{x^2}{2R} \quad |x| < c \tag{1}$$

where Δ and θ_0 are the beam upper surface displacement and rotation under the indenter. The end support conditions that need to be satisfied are zero slope and displacement at $x = -L_0$ and zero shear and moment at $x = L_1 = L - L_0$.

By applying these end support conditions to the generalized elasticity solution, we obtain a system of equations for the quantities M_0, M_1, a_0, and a_1 in terms of unknown functions $E_S(\xi)$ and $E_A(\xi)$. These

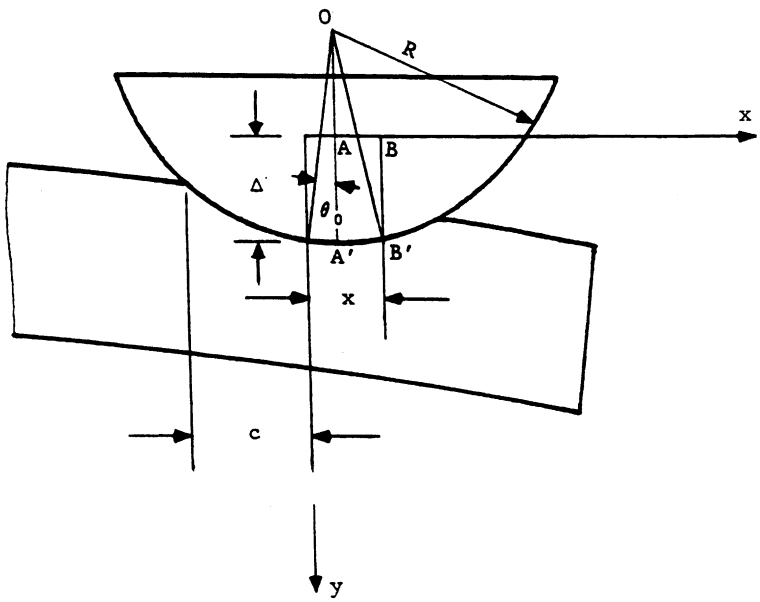

Fig. 2. Geometric parameters at the contact site.

functions are determined by applying the boundary condition at the contact site given by Eq. (1) to the generalized elasticity solution presented in the preceding section. Following established procedures, we arrive at the following governing equations for the static indentation of a cantilever beam in terms of $E_S(\xi)$ and $E_A(\xi)$:

$$-\frac{1-v}{\mu}\int_0^\infty \frac{E_A(\xi)[1-\cos(\xi x)]}{\beta^2-\mathrm{sh}^2\beta}(\beta+\mathrm{sh}\,\beta\,\mathrm{ch}\,\beta)\,\mathrm{d}\xi-\frac{M_1-M_0}{2DL}x^2=0 \tag{2}$$

$$-\frac{1-v}{\mu}\int_0^\infty \frac{E_S(\xi)\sin(\xi x)}{\beta^2-\mathrm{sh}^2\beta}(\beta+\mathrm{sh}\,\beta\,\mathrm{ch}\,\beta)\,\mathrm{d}\xi-\frac{x}{D}\left(M_0+\frac{M_1-M_0}{L}L_0\right)=-\frac{x}{R} \tag{3}$$

where $D=\mu h^3/6(1-v)$. Eqs. (2) and (3) are coupled Fredholm integral equations of the first kind and as such their solutions are ill conditioned. To facilitate the numerical treatment of this indentation problem, the integral transform method developed by Keer and Miller (1983) is used to convert Eqs. (2) and (3) into the following two coupled Fredholm integral equations of the second kind (whose solutions are much more stable):

$$\frac{h^3}{6}\psi(x)+\int_0^c \psi(t)K_1(x,t)\,\mathrm{d}t+\int_0^c \phi(t)K_2(x,t)\,\mathrm{d}t=-\frac{Dx}{R} \tag{4}$$

$$\frac{h^3}{6}\phi(x)+\frac{h^3}{6}\int_0^x \frac{\phi(t)}{t}\,\mathrm{d}t+\int_0^c \psi(t)K_3(x,t)\,\mathrm{d}t+\int_0^c \phi(t)K_4(x,t)\,\mathrm{d}t=0 \tag{5}$$

where

$$E_S(\xi)=\int_0^c \psi(t)J_0(\xi t)\,\mathrm{d}t \tag{6}$$

$$E_A(\xi)=\int_0^c \phi(t)J_1(\xi t)\,\mathrm{d}t \tag{7}$$

and the kernels K_1 through K_4 are given as follows:

$$K_1(x,t)=-\int_0^\infty\left[\frac{h^3}{6}\left(\frac{\beta+\mathrm{sh}\,\beta\,\mathrm{ch}\,\beta}{\beta^2-\mathrm{sh}^2\beta}+1\right)\xi x J_0(\xi x)+\frac{x}{\xi^2}\cos(\xi L_1)\right]J_0(\xi t)\,\mathrm{d}\xi-\frac{\pi}{2}xL_1 \tag{8}$$

$$K_2(x,t)=-\frac{\pi}{4}xt \tag{9}$$

$$K_3(x,t)=\frac{3\pi}{8}x^2 \tag{10}$$

$$K_4(x,t)=\frac{h^3}{6}\int_0^\infty\left(\frac{\beta+\mathrm{sh}\,\beta\,\mathrm{ch}\,\beta}{\beta^2-\mathrm{sh}^2\beta}+1\right)[J_0(\xi x)-\xi x J_1(\xi x)-1]J_1(\xi t)\,\mathrm{d}\xi \tag{11}$$

where $\mathrm{sh}\,\beta=\sinh\beta$ and $\mathrm{ch}\,\beta=\cosh\beta$.

Once Eqs. (4) and (5) are solved for $\psi(x)$ and $\phi(x)$, all necessary physical quantities may be calculated. For example, the displacement under the indenter, i.e., $\Delta=u_y(0,0)$, is given in terms of $\psi(x)$ and $\phi(x)$ by the following expression:

$$\Delta=\int_0^c \psi(t)K_5(t)\,\mathrm{d}t+\int_0^c \phi(t)K_6(t)\,\mathrm{d}t \tag{12}$$

where

$$K_5(t) = \frac{h^3}{6D}\int_0^\infty \left[\left(\frac{\beta+\operatorname{sh}\beta\operatorname{ch}\beta}{\beta^2-\operatorname{sh}^2\beta}+1\right)\frac{1-\cos(\xi L_0)}{\xi} - \frac{L_0}{\beta-\operatorname{sh}\beta}\sin(\xi L_0) - \frac{3L_0^2}{h^3}\frac{\cos(\xi L_1)}{\xi^2}\right]J_0(\xi t)\,\mathrm{d}\xi - \frac{\pi L_0}{12D}\left[L_0(3L-L_0) - \frac{\nu h^2}{2(1-\nu)}\right] - \frac{h^3}{6D}\cosh^{-1}\left(\frac{L_0}{t}\right) + \frac{\pi(3-2\nu)h^2}{24(1-\nu)D}L_0 \tag{13}$$

$$K_6(t) = \int_0^\infty \frac{h^3}{6D}\left[\left(\frac{\beta+\operatorname{sh}\beta\operatorname{ch}\beta}{\beta^2-\operatorname{sh}^2\beta}+1\right)\frac{\sin(\xi L_0)}{\xi} - \frac{L_0}{\beta-\operatorname{sh}\beta}\cos(\xi L_0)\right]J_1(\xi t)\,\mathrm{d}\xi - \frac{h^3}{6D}\frac{t}{L_0+\sqrt{L_0^2-t^2}} - \frac{\pi L_0^2}{8D}t \tag{14}$$

While Eq. (14) is identical to the corresponding equation in Zhou and Schonberg (1995), Eq. (13) has an additional term within the second set of brackets. This extra term is due to the application of the generalized elasticity solution for $\bar{\theta}$ developed herein. Additionally, the average slope of the beam $\bar{\theta}(x)$ is found to be given by the following expression:

$$\bar{\theta}(x;|x|\leqslant c) = \int_0^c \psi(t)K_7(x,t)\,\mathrm{d}t + \int_0^c \phi(t)K_8(x,t)\,\mathrm{d}t \tag{15}$$

$$K_7(x,t) = -\frac{1}{D}\int_0^\infty \left[\frac{h^3}{6}\frac{\sin(\xi x)+\sin(\xi L_0)}{\beta-\operatorname{sh}\beta} + (L_0+x)\frac{\cos(\xi L_1)}{\xi^2}\right]J_0(\xi t)\,\mathrm{d}\xi - \frac{\pi}{2D}\left[L_0\left(L-\frac{L_0}{2}\right)+x(L-L_0)-\frac{x^2}{2}\right] + \frac{\pi h^2}{24D}\frac{3-2\nu}{1-\nu} + \operatorname{sgn}(x)\frac{h^2}{12D}\frac{3-2\nu}{1-\nu} \times \left[\frac{\pi}{2}\int_0^{|x|}\psi(t)\,\mathrm{d}t + \int_{|x|}^c \psi(t)\sin^{-1}\left(\frac{|x|}{t}\right)\mathrm{d}t\right] \tag{16}$$

$$K_8(x,t) = \frac{h^3}{6D}\int_0^\infty \frac{\cos(\xi x)-\cos(\xi L_0)}{\beta-\operatorname{sh}\beta}J_1(\xi t)\,\mathrm{d}\xi - \frac{\pi}{4D}(L_0+x)t - \frac{h^2}{12D}\frac{3-2\nu}{1-\nu}\int_{|x|}^c \frac{\phi(t)}{t}\sqrt{t^2-x^2}\,\mathrm{d}t \tag{17}$$

To assess the validity of the elasticity solution presented herein, its predictions for beam displacement and rotation under the indenter are compared with the predictions of a beam theory solution that uses as input the contact pressure distribution generated by the elasticity solution developed herein. Such beam theory expressions for displacement and rotation are written as follows:

$$\Delta_{\mathrm{B}} = \frac{L_0^2}{6D}\int_{-c}^c p(s)(2L_0+3s)\,\mathrm{d}s - \frac{1}{6D}\int_{-c}^0 s^3 p(s)\,\mathrm{d}s \tag{18}$$

$$\theta_{\mathrm{B}}(x) = \frac{1}{2D}\int_{-c}^c p(s)(L_0+s)^2\,\mathrm{d}s - \frac{1}{2D}\int_x^c p(s)(x-s)^2\,\mathrm{d}s \tag{19}$$

where $p(s) = -\sigma_{yy}(s,0)$ is the contact pressure distribution forthcoming as part of the solution to the static indentation problem.

3.1. Results and discussion

Solutions to the static indentation problem are obtained for $c/h = 0.2$, 0.5, and 1.0, $L/h = 10$ and 20, and for each L/h, $L_0/L = 0.25$, 0.5 and 0.75. Of particular interest are the results obtained for beam displacement and rotation. These results are presented in Table 1 and discussed in detail in the following paragraphs.

Table 1
Non-dimensional displacement and rotation comparisons: new model, beam theory and old model (Zhou and Schonberg, 1995)

L/h		$L_0/L = 0.25$			$L_0/L = 0.50$			$L_0/L = 0.75$			c/h
		New model	Beam theory	Old model	New model	Beam theory	Old model	New model	Beam theory	Old model	
10	Displacement	2.0	2.0	2.0	16.1	16.1	16.1	54.3	54.3	54.3	0.2
		15.5	15.7	15.6	126.4	126.7	126.6	428.6	429.2	429.2	0.5
		365.3	376.8	378.4	3356.5	3373.7	3374.5	11782.9	11805.8	11784.0	1.0
10	Rotation	1.2	1.2	–	4.8	4.8	–	10.9	10.9	–	0.2
		9.4	9.4	–	38.0	37.9	–	85.7	85.7	–	0.5
		214.6	217.6	–	982.5	985.5	–	2312.9	2315.9	–	1.0
20	Displacement	16.0	16.1	16.1	128.7	128.7	128.7	434.3	434.5	434.4	0.2
		126.4	126.7	126.4	1018.3	1019.1	1019.4	3444.2	3445.3	3435.1	0.5
		3300.0	3317.2	3473.6	28458.6	28487.0	28669.8	97802.3	97842.0	98185.0	1.0
20	Rotation	4.8	4.8	–	19.3	19.3	–	43.5	43.4	–	0.2
		38.0	37.9	–	152.7	152.6	–	344.2	344.1	–	0.5
		966.0	969.0	–	4206.0	4209.0	–	9679.4	9682.3	–	1.0

If we compare the displacement and rotation predictions of the elasticity solution developed herein and the predictions of the beam theory solution given, we see that the two solutions agree very well. This agreement improves for displacement and rotation as L_0/L increases, for displacement as c/h decreases, and for rotation as c/h increases. This can be explained by the following considerations. First, as L_0/L increases, the effects of shear deformation on beam response become negligible. While the elasticity solution incorporates those effects, the beam theory solution does not. Therefore, these two solutions will match more closely for indenter locations that result in minimal shear deformations. Second, for displacements, as c/h decreases the local effects of beam upper surface deformation become negligible. Again, while the elasticity solution incorporates those effects, the beam theory solution does not. Therefore, these two solutions will match more closely in displacement prediction for smaller c/h values. Finally, for rotations, c/h increases, the local effects of indenter curvature on beam upper surface deformation become negligible. While the elasticity solution incorporates those effects, the beam theory solution does not. Therefore, these two solutions will match more closely in rotation prediction for larger c/h values.

Table 1 also shows a comparison between the displacement predictions of the new model developed herein, which includes second-order shear effects, and the displacement predictions obtained by Zhou and Schonberg (1995), which did not. We see that for small values of c/h the two solutions agree quite well. However, for $c/h \geqslant 1$ and for small values of L_0/L the two solutions differ noticeably. This is again explained by noting that as c/h decreases and L_0/L increases, the shear effects of cantilever beam become negligible. While the current model incorporates those effects, the previous model does not. Therefore, these two models will match more closely for smaller contact area and indenter locations that result in minimal shear effects.

4. Low velocity impact of a cantilever beam

In this section we examine the normal low velocity impact of a frictionless rigid cylindrical projectile on an isotropic cantilever beam. The geometry of the problem is shown in Fig. 2. Only low velocity impact is considered in order to avoid complications that may result from high velocity impact, such as penetration

or puncture. The constraints imposed on the problem ensure that the projectile will rebound along the vertical line defining its incoming trajectory. As such, it can be argued that the physical problem being modeled is that of a rotating hammer with a cylindrical nose impacting a cantilever beam.

The development of the dynamic indentation problem being considered is based on that developed by Zhou and Schonberg (1994), which is itself a modification of the low velocity impact models developed by Keer and Lee (1985) and Schonberg et al. (1987). The idea behind the modifications proposed by Zhou and Schonberg (1994) was that only the relative static beam upper-surface deformation with respect to the dynamic beam deflection (rather that the total static beam upper-surface deformation) should be superposed on a dynamic beam theory solution to obtain the timevarying load–displacment relationship. This modification was motivated by the fact that the dynamic beam theory solution defining beam displacement consists of the time-dependent part of the beam response relative to an instantaneous static equilibrium position and the static response of the beam that defines the instantaneous static equilibrium position at current loading. The relative beam upper-surface deformation is extracted from the total static elastic layer displacement solution by subtracting a static beam theory displacement solution from a static finite length elastic layer displacement solution.

As a result, the formulation of the dynamic contact problem consists of three types of solutions: (1) a static elastic finite layer solution, which is obtained by applying the beam support conditions to the generalized static elastic layer solution presented previously; (2) a dynamic solution, which is obtained from a standard beam vibration analysis; and (3) a static beam theory solution, which is used to cancel out the static part of the beam vibration solution that describes the instantaneous beam equilibrium position. Superposition of the three solutions and the matching of boundary conditions lead to a Volterra integral equation of the second kind. The unknown contact region and pressure distribution at each instant of time are obtained using a technique developed by Ahmadi et al. (1983) for the solution of non-Hertzian contact problems.

We note that in the case of symmetric impact or in the case of static indentation just considered, the contact length can be taken to be symmetric with respect to the static contact center. However, in the case of asymmetric impact now being considered, the two half-contact lengths are not necessarily symmetric and are actually obtained as part of the solution to the impact problem. As such, in Fig. 2 and in the development that follows, the total contact length is divided amongst two unequal contact lengths c_1 and c_2, one on either side of the coordinate axis defining the impact trajectory.

4.1. Static elastic finite layer displacement solution

Following the procedure in Zhou and Schonberg (1994), we focus on deriving an expression for transverse beam deflection that will serve as the basis for the governing equation of motion ultimately obtained. By applying the end support conditions for a cantilever beam to the generalized elasticity for a finite layer, we again obtain a system of equations that are used to solve for end moments and unknown constants. After collecting terms and adjusting the asymptotic behavior of the kernel of the resulting integrand, we obtain, after some simplification, the following expression for transverse displacement $u_y(x,0)$:

$$u_y(x,0) = \frac{1}{\pi D}\int_{c_1}^{c_2} p(x')K(x,x')\,\mathrm{d}x' - \frac{h^3}{6\pi D}\int_{c_1}^{c_2} p(x')\ln\left(\frac{|x-x'|}{L_0+x'}\right)\mathrm{d}x' + \frac{L_0+x}{4D}\left[L(L_0+x)(L_1-x) - \frac{1}{3}(L_0+x)^2 + \frac{(1+\nu)h^2}{6(1-\nu)}\right]\int_{c_1}^{c_2} p(x')\,\mathrm{d}x' \tag{20}$$

where

$$K(x,x') = \int_0^\infty \left\{ -\frac{h^3}{6}\left(\frac{\beta + \operatorname{sh}\beta \operatorname{ch}\beta}{\beta^2 - \operatorname{sh}^2\beta} + 1\right)\frac{\cos[\xi(x-x')] - \cos[\xi(L_0+x')]}{\xi} + \frac{(L_0+x)h^3}{12(1-\nu)}\frac{\sin[\xi(L_0+x')]}{\beta - \operatorname{sh}\beta} + \frac{(L_0+x)^2}{2}\frac{\cos[\xi(L_1-x')]}{\xi^2}\right\} \mathrm{d}\xi \tag{21}$$

4.2. Static beam theory displacement solution

Using elementary engineering mechanics, the beam theory solution for a cantilever beam subjected to an arbitrary normal loading at its upper surface is written as follows:

$$u_y^{\mathrm{B}}(x) = \frac{1}{6D}\int_x^{c_2} p(x')(L_0+x)^2(2L_0+3x'-x)\,\mathrm{d}x' + \frac{1}{6D}\int_{c_1}^{x} p(x')(L_0+x')^2(2L_0+3x-x')\,\mathrm{d}x' \tag{22}$$

4.3. Dynamic beam theory displacement solution

By using a Laplace transform technique and a normal mode expansion (see, e.g., Graff, 1975), we find that for the case of zero initial conditions the dynamic beam deflection is given by

$$u_y(x,t) = \frac{1}{\rho h}\sum_{n=1}^{\infty}\frac{Y_n(L_0+x)}{a\beta_n^2}\int_0^L Y_n(L_0+u)\,\mathrm{d}u\int_0^t p(u,\tau)\sin a\beta_n^2(t-\tau)\,\mathrm{d}\tau \tag{23}$$

where $a = \sqrt{D/\rho h}$, ρ is the mass density,

$$Y_n(x) = F_n\left[\frac{\operatorname{ch}(\beta_n x) - \cos(\beta_n x)}{\operatorname{ch}(\beta_n L) + \cos(\beta_n L)} - \frac{\operatorname{sh}(\beta_n x) - \sin(\beta_n x)}{\operatorname{sh}(\beta_n L) + \sin(\beta_n L)}\right] \tag{24}$$

and

$$F_n = 1\Big/\sqrt{\int_0^L Y_n^2(x)\,\mathrm{d}x} = \frac{\operatorname{ch}(\beta_n L) + \cos(\beta_n L)}{\sqrt{L}} \tag{25}$$

For a cantilever beam, the frequency equation is given as

$$\cos(\beta_n L)\operatorname{ch}(\beta_n L) = -1 \tag{26}$$

4.4. Governing equation of motion

As discussed previously, the total dynamic displacement is given by the addition of Eqs. (20) and (23) followed by the subtraction of Eq. (22) with the following result:

$$u_y(x,0,t) = \frac{1}{\pi D}\int_{c_1(t)}^{c_2(t)} p(x',t)K(x,x')\,\mathrm{d}x' - \frac{h^3}{6\pi D}\int_{c_1(t)}^{c_2(t)} p(x',t)\ln\left(\frac{|x-x'|}{L_0+x'}\right)\mathrm{d}x'$$
$$+\frac{L_0+x}{4D}\left[L(L_0+x)(L_1-x) - \frac{1}{3}(L_0+x)^2 + \frac{(1+\nu)h^2}{6(1-\nu)}\right]\int_{c_1(t)}^{c_2(t)} p(x',t)\,\mathrm{d}x'$$
$$-\left\{\frac{1}{6D}\int_x^{c_2(t)} p(x',t)(L_0+x)^2(2L_0+3x'-x)\,\mathrm{d}x' + \frac{1}{6D}\int_{c_1(t)}^{x} p(x',t)(L_0+x')^2(2L_0+3x-x')\,\mathrm{d}x'\right\}$$
$$+\frac{1}{\rho h}\int_0^t\int_{c_1(\tau)}^{c_2(\tau)} p(x',\tau)\sum_{n=1}^{\infty}\frac{Y_n(L_0+x)Y_n(L_0+x')}{a\beta_n^2}\sin a\beta_n^2(t-\tau)\,\mathrm{d}x'\,\mathrm{d}\tau \tag{27}$$

In the contact region we have

$$u_y(x,0,t) = \Delta(t) - \frac{x^2}{2R} \quad c_1(t) < x < c_2(t) \tag{28}$$

where $\Delta(t)$ is the approach of the projectile (a function of time, as are the contact region boundaries c_1 and c_2), and R is the radius of curvature of the projectile. An additional equation is obtained from Newton's equation of motion

$$m_{\mathrm{p}}\frac{\partial^2\Delta}{\partial t^2} = -\int_{c_1(t)}^{c_2(t)} p(x,t)\,\mathrm{d}x \tag{29}$$

where m_{p} is the mass of the projectile per unit length. If the projectile has an initial velocity V, then Eq. (29) can be integrated twice to yield

$$\Delta(t) = Vt - \frac{M}{\rho hL}\int_0^t (t-\tau)\int_{c_1(\tau)}^{c_2(\tau)} p(x',\tau)\,\mathrm{d}x'\,\mathrm{d}\tau \tag{30}$$

where M is the ratio of the mass of the beam to that of the projectile. Substituting Eqs. (27) and (30) into Eq. (28) and rearranging terms yield the integral equation for the impact problem

$$\frac{1}{\pi D}\int_{c_1(t)}^{c_2(t)} p(x',t)\widetilde{K}(x,x')\,\mathrm{d}x' + \frac{1}{D}\int_{c_1(t)}^{c_2(t)} p(x',t)L(x,x')\,\mathrm{d}x' + \frac{1}{\rho h}\int_0^t\int_{c_1(\tau)}^{c_2(\tau)} p(x',\tau)N(x,x',\tau)\,\mathrm{d}x'\,\mathrm{d}\tau$$
$$+\frac{M}{\rho hL}\int_0^t (t-\tau)\int_{c_1(\tau)}^{c_2(\tau)} p(x',\tau)\,\mathrm{d}x'\,\mathrm{d}\tau = Vt - x^2/2R \tag{31}$$

where

$$\widetilde{K}(x,x') = \int_0^{\infty}\left\{-\frac{h^3}{6}\left(\frac{\beta+\mathrm{sh}\,\beta\,\mathrm{ch}\,\beta}{\beta^2-\mathrm{sh}^2\beta}+1\right)\frac{\cos[\xi(x-x')]-\cos[\xi(L_0+x')]}{\xi}\right.$$
$$\left.+\frac{(L_0+x)h^3}{12(1-\nu)}\frac{\sin[\xi(L_0+x')]}{\beta-\mathrm{sh}\,\beta}+\frac{(L_0+x)^2}{2}\frac{\cos[\xi(L_1-x')]}{\xi^2}\right\}\mathrm{d}\xi$$
$$+\frac{\pi}{4}(L_0+x)\left[L(L_0+x)(L_1-x)-\frac{1}{3}(L_0+x)^2+\frac{(1+\nu)h^2}{6(1-\nu)}\right] \tag{32}$$

$$L(x,x') = -\frac{h^3}{6\pi D}\int_{c_1}^{c_2} p(x')\ln\left(\frac{|x-x'|}{L_0+x'}\right)\mathrm{d}x' - \frac{1}{6D}\left[(L_0+x)^2(2L_0+3x'-x)H(x'-x)H(x-x') + (L_0+x')^2(2L_0+3x-x')H(x-x')\right] \tag{33}$$

$$N(x,x',\tau) = \sum_{n=1}^{\infty}\frac{Y_n(L_0+x)Y_n(L_0+x')}{a\beta_n^2}\sin a\beta_n^2(t-\tau) \tag{34}$$

We note that the first term in Eq. (33) represents the local indentation behavior of the beam while the second term allows only the static finite elastic layer solution to describe the instantaneous beam equilibrium position. As observed previously by Zhou and Schonberg (1994), inclusion of this term significantly improves the accuracy of the predictions of the original analytical model for center impact of a simply supported beam.

4.5. Elementary beam theory solution

An elementary beam theory analysis (Goldsmith, 1960) yields the following expressions for maximum transverse displacement and impact duration:

$$u_{y,\max} = V\tau/\sqrt{(\varepsilon M+1)M} \tag{35}$$

$$t_0 = \pi\tau\sqrt{(\varepsilon M+1)/M} \tag{36}$$

where $\tau = \sqrt{\rho hL/k}$ and V, M are as defined previously. For a cantilever beam, the values of ε and k are given as follows:

$$\varepsilon = \frac{33}{140}\left(\frac{L_0}{L}\right) + \left(\frac{L_0}{36L}\right)\left[\left(\frac{3L}{L_0}-1\right)^3 - 8\right] \tag{37}$$

$$k = \frac{3D}{L_0^3} \tag{38}$$

4.6. Results and discussion

The material and geometric parameters used to evaluate our low velocity impact model are listed in Table 2. Solutions were obtained for cantilever end support conditions for three impact locations ($L_0/L = 0.6$, 0.4,

Table 2
Material and geometric parameters

	Test set 1, $L_0/L = 0.6$	Test set 2, $L_0/L = 0.4$	Test set 3, $L_0/L = 0.2$
Material	Castolite	Castolite	Castolite
E (N/m^2)	4.827×10^9	4.827×10^9	4.827×10^9
υ	0.355	0.355	0.355
ρ (Kg/m^3)	1212	1212	1212
R (cm)	1.93	1.93	1.93
L (cm)	12.70	12.70	12.70
L_0 (cm)	7.62	5.08	2.54
h (cm)	1.93	1.93	1.93

and 0.2), for two impact velocities ($V = 1$, 5 m/s), and for three mass ratios ($M = 0.5$, 1, 2). Highlights of the results obtained in this parametric study are presented in Tables 3–5 and in Figs. 3 and 4, and are discussed below in detail.

Table 3 shows that as M increases (corresponding to the situation of using the same beam but lighter projectiles), the normal peak stresses under the indenter and maximum contact length decrease for all three test sets. This is because when $M < 1$, that is, the projectile is more massive that the beam, the lighter beam must transmit a much larger force to the heavier projectile during rebound in order to successfully reverse its trajectory. This results in larger normal peak stresses and maximum contact lengths. It is also seen in these tables that the maximum normal peak stresses and corresponding contact lengths increase significantly and non-linearly when impact locations move toward the end support. This is because both the effective transverse stiffness and the "whipping" effect of the beam increases significantly as the impact location moves toward the end support.

Table 3
Maximum contact stresses and contact lengths

	M	Peak normal stress under the indenter ($\times 10^7$ N m^{-2})			Maximum contact length (mm)		
		Test set 1, $L_0/L = 0.6$	Test set 2, $L_0/L = 0.4$	Test set 3, $L_0/L = 0.2$	Test set 1, $L_0/L = 0.6$	Test set 2, $L_0/L = 0.4$	Test set 3, $L_0/L = 0.2$
$V = 1$ m/s	0.5	5.139	5.302	6.893	0.711	0.762	1.016
	1.0	4.317	4.501	5.680	0.610	0.610	0.813
	2.0	3.883	4.357	4.831	0.559	0.610	0.711
$V = 5$ m/s	0.5	10.935	11.521	15.559	1.524	1.626	2.235
	1.0	9.860	10.279	12.854	1.372	1.473	1.829
	2.0	8.816	9.955	10.928	1.270	1.372	1.575

Table 4
Maximum transverse displacement under the indenter (mm)

	M	Test set 1, $L_0/L = 0.6$		Test set 2, $L_0/L = 0.4$		Test set 3, $L_0/L = 0.2$	
		Elasticity	Beam theory	Elasticity	Beam theory	Elasticity	Beam theory
$V = 1$ m/s	0.5	0.423	0.415	0.217	0.176	0.059	0.034
	1.0	0.312	0.253	0.129	0.098	0.032	0.017
	2.0	0.189	0.145	0.083	0.053	0.021	0.009
$V = 5$ m/s	0.5	2.100	2.212	1.096	0.881	0.291	0.169
	1.0	1.552	1.263	0.660	0.492	0.162	0.087
	2.0	0.948	0.725	0.410	0.263	0.108	0.044

Table 5
Duration of impact ($\times 10^{-3}$ s)

	M	Test set 1, $L_0/L = 0.6$		Test set 2, $L_0/L = 0.4$		Test set 3, $L_0/L = 0.2$	
		Elasticity	Beam theory	Elasticity	Beam theory	Elasticity	Beam theory
$V = 1$ m/s	0.5	1.275	2.005	0.450	1.400	0.350	0.914
	1.0	1.450	1.647	0.300	1.254	0.175	0.887
	2.0	1.450	1.435	0.300	1.174	0.150	0.873
$V = 5$ m/s	0.5	1.275	2.005	0.450	1.400	0.350	0.914
	1.0	1.450	1.647	0.300	1.254	0.175	0.887
	2.0	1.450	1.435	0.300	1.174	0.150	0.873

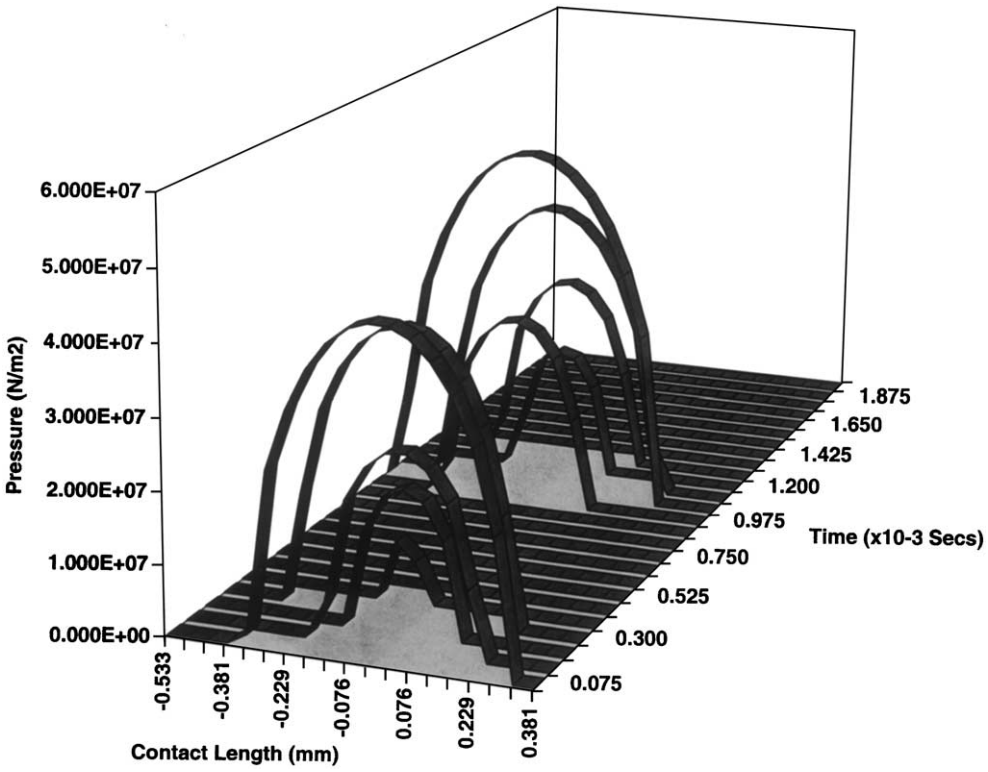

Fig. 3. Contact pressure time history; $L_0/L = 0.6$, $M = 0.5$, $V = 1$ m/s.

Tables 4 and 5 show the maximum beam transverse displacement under indenter and the impact duration as functions of mass ratio and impact velocity of the projectile as well as impact location. A comparison of the predictions of the model developed herein and the elementary beam theory model reveals large discrepancies, especially for impact duration. This is because multiple impacts and early final separation occur in cantilever beam impact case even when mass ratio is small. The discrepancies between the two models for maximum transverse displacement increase when mass ratios increase: when mass ratios are larger, smaller projectile mass leads to earlier final separation. In addition, the maximum transverse displacement occurs when beam and projectile have separated. The discrepancies also increase when the impact location moves toward the end support. This is also expected because the closer the impact location moves toward the support, the stronger the "whipping" effect from the free end of the beam becomes. This results in the large discrepancies in the maximum displacement that occur when the projectile and the beam have separated. Because of this, it is apparent that the assumption of the elementary beam theory impact model that the dynamic transverse displacement is geometrically similar to the static displacement curve is no longer valid.

Table 4 also shows that trends of transverse displacement predictions for different impact locations are similar in nature: maximum transverse displacements are found to increase as mass ratio decreases. A similar trend is observed with respect to the dependence of maximum beam displacement and contact force on impact velocity: the amplitudes are seen to be approximately proportional to the relative values of the initial impact velocities. This is in agreement with elementary beam theory predictions and the numerical results obtained by Schonberg et al. (1987). Finally, it is seen that for cantilever beam impact, the impact

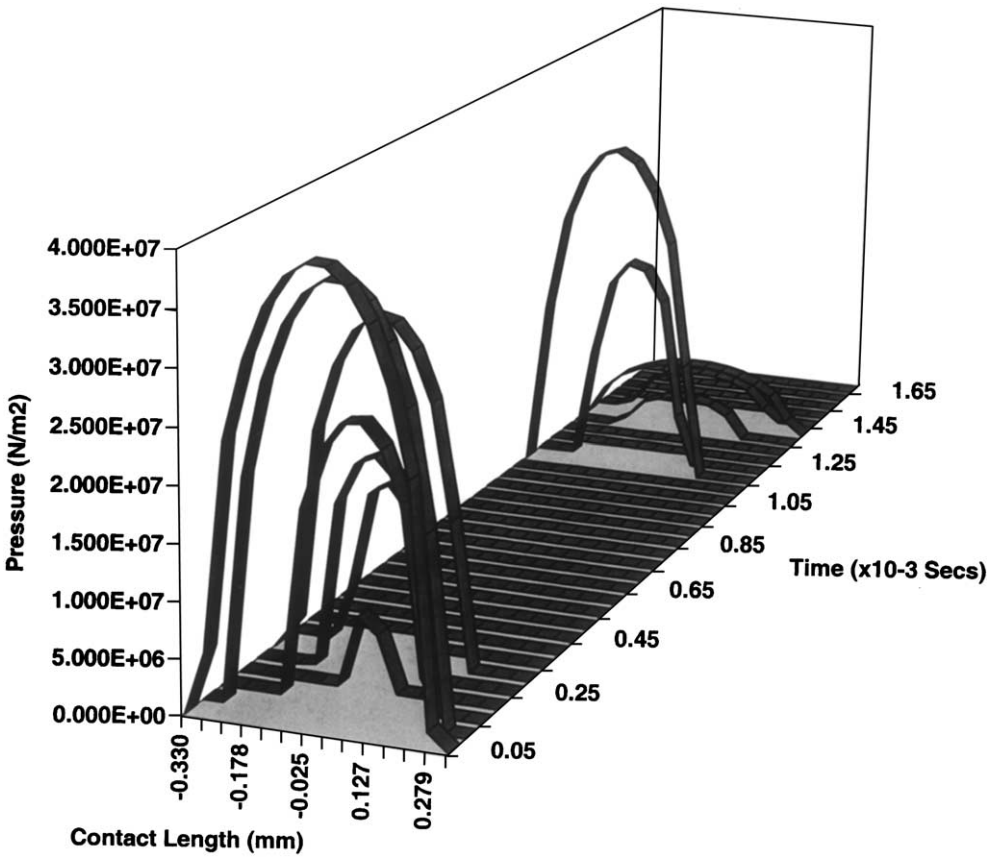

Fig. 4. Contact pressure time history; $L_0/L = 0.6$, $M = 1.0$, $V = 1$ m/s.

duration is again virtually independent of the initial impact velocity as was also shown previously in simply supported and fixed–fixed beam impact cases by Schonberg et al.

It is also interesting to note in Table 5 that the closer the impact location moves toward the fixed end support, the shorter the impact duration becomes. This is because when the impact location is closer to the end support, the beam is less likely to catch the projectile for double impact during rebounding. This leads to an earlier final separation. It is also noted that for impact locations close to the free end, the impact duration does not increase monotonously as mass ratio decreases, which is contrary to beam theory predictions. This is because the "whipping" effects of the beam's free end allow the beam to catch the projectile for multiple impact during rebound. A large mass ratio (lighter projectile versus same beam) was found to create as many as three impacts and thereby resulted in longer impact durations.

Figs. 3 and 4 show the normal contact stress distribution histories for $M = 0.5$ and 1 for the impact location $L_0/L = 0.6$. Evident in these figures is the receding contact phenomenon, which is characterized by a moving contact center. This phenomenon is more evident for $M = 0.5$ than for $M = 1$ because for a smaller mass ratio the dynamic contact is localized and centered about the impact location. Further examination and comparison of Figs. 3 and 4 reveals two additional features. First, both figures show final separation occurs when the beam is below its initial horizontal position. Second, Fig. 3 shows double impact while Fig. 4 shows a triple impact. The multiple impact phenomenon for cantilever beam can be considered as a combined result of the beam's transverse stiffness and the "whipping" effect of the free end.

The beam's low transverse stiffness allows smaller contact force to rebound the projectile while the "whipping" effect allows larger amplitude of beam displacement to catch the projectile during its rebounding course.

5. Summary and assessment

In the first part of this paper, the static cantilever beam indentation problem is reformulated and successfully solved using a generalized elasticity solution and modified boundary conditions at the contact site that include beam upper surface rotation effects. In the second part, the asymmetric low velocity cantilever beam impact problem is also successfully reformulated and solved.

It would appear that the major limitation of the models presented herein is that their predictions of beam response are valid only when the contact zone is sufficiently far away from end supports. Improvement in the predictions of beam indentation and low velocity impact responses can be achieved by using a more precise superposition solution in which the boundary conditions at end supports are satisfied in terms of stresses instead of moments and shears. Ultimately, experimental validation and correlation are required to assess the predictive accuracy of the models developed herein to facilitate their application to real word problems (e.g., finding the "sweet spot" on a baseball bat) and to direct future research efforts in beam contact and impact analysis.

References

Ahmadi, N., Keer, L.M., Mura, T., 1983. Non-Hertzian stress analysis—normal and sliding contact. International Journal of Solids and Structures 19, 357–373.

Goldsmith, W., 1960. Impact: The Theory and Physical Behavior of Colliding Solids. Edward Arnold, London.

Graff, K.F., 1975. Wave Motion in Elastic Solids. Ohio State University Press, Columbus, OH.

Keer, L.M., Lee, J.C., 1985. Dynamic impact of an elastically supported beam—large area contact. International Journal of Engineering Science 23, 987–997.

Keer, L.M., Miller, G.R., 1983. Smooth indentation of a finite layer. Journal of Engineering Mechanics 109, 706–717.

Keer, L.M., Schonberg, W.P., 1986a. Smooth indentation of an isotropic cantilever beam. International Journal of Solids and Structures 22, 87–106.

Keer, L.M., Schonberg, W.P., 1986b. Smooth indentation of a transversely isotropic cantilever beam. International Journal of Solids and Structures 22, 1033–1053.

Schonberg, W.P., Keer, L.M., Woo, T.K., 1987. Low velocity impact of transversely isotropic beams and plates. International Journal of Solids and Structures 23, 871–896.

Zhou, M., Schonberg, W.P., 1994. Comment on global/local method for low-velocity impact problems. Journal of Engineering Mechanics 120, 1042–1056.

Zhou, M., Schonberg, W.P., 1995. Rotation effects in the global/local analysis of cantilever beam contact problems. Acta Mechanica 108, 49–62.

Zhou, M., Schonberg, W.P., 2001. Smooth asymmetric two-dimensional indentation of a finite elastic beam. Journal of Applied Mechanics 68 (1), 357–360.